



HAL
open science

Acoustic metastructure for effective low-frequency acoustic energy harvesting

Ming Yuan, Ziping Cao, Jun Luo, Roger Ohayon

► **To cite this version:**

Ming Yuan, Ziping Cao, Jun Luo, Roger Ohayon. Acoustic metastructure for effective low-frequency acoustic energy harvesting. *Journal of Low Frequency Noise, Vibration and Active Control*, 2018, 37 (4), pp.1015-1029. 10.1177/1461348418794832 . hal-03177087

HAL Id: hal-03177087

<https://hal.science/hal-03177087v1>

Submitted on 23 Nov 2021

HAL is a multi-disciplinary open access archive for the deposit and dissemination of scientific research documents, whether they are published or not. The documents may come from teaching and research institutions in France or abroad, or from public or private research centers.

L'archive ouverte pluridisciplinaire **HAL**, est destinée au dépôt et à la diffusion de documents scientifiques de niveau recherche, publiés ou non, émanant des établissements d'enseignement et de recherche français ou étrangers, des laboratoires publics ou privés.



Distributed under a Creative Commons Attribution 4.0 International License

Acoustic metastructure for effective low-frequency acoustic energy harvesting

Journal of Low Frequency Noise,
Vibration and Active Control
2018, Vol. 37(4) 1015–1029
© The Author(s) 2018
DOI: 10.1177/1461348418794832
journals.sagepub.com/home/lfn



Ming Yuan¹ , Ziping Cao², Jun Luo² and Roger Ohayon³

Abstract

In this study, a multifunctional acoustic metastructure is proposed to achieve both effective low-frequency sound isolation and acoustic energy harvesting. A metallic substrate with proof mass is adopted to generate the local resonant phenomenon for the purpose of overcoming the drawbacks of the previous rubber film-based acoustic metastructure; the latter usually requires an elaborate tension process. Numerical simulations show that the proposed structure exhibits excellent noise isolation performance in the low-frequency band. Meanwhile, the incident sound energy can be converted into electrical energy with the help of an added piezoelectric patch. Numerical simulation results indicate that the harvested energy can reach the mW level. The parameters' influence on the metastructure's vibro-acoustic and energy harvesting performance are discussed in detail. An optimized configuration is selected and used for experimental study. It is demonstrated that 0.21 mW electrical power at 155 Hz can be harvested by the proposed metastructure under 114 dB sound pressure excitation.

Keywords

Low-frequency noise, acoustic energy harvesting, acoustic metamaterial

Introduction

Low-frequency noise isolation or attenuation has always been a focus of scientific research and industrial engineering. Very significant amounts of this band of noise are emitted by industrial plants, transportation vehicles, and civic buildings. Typical noise sources include pumps, electric motors, electric transformers, cooling towers, and traffic vehicles. In the low-frequency range, the wavelength of sound waves can be meters long, which transmits through thin-walled structures easily without remarkable attenuation.¹ Accordingly, it is important to investigate effective low-frequency noise control methods.

Previous studies have demonstrated that an active noise control,² or active structural acoustic control approach,³ can suppress the low-frequency noise effectively. However, the active control system cost is high and suffers from system stability problems.

The acoustic metamaterials or subwavelength acoustic metasurfaces open a new way to manipulate acoustic waves, which can be used for wave-steering,⁴ realizing generalized Snell's law⁵ and low-frequency noise insulation.⁶ As reported in the low-frequency noise insulation application, it was found that the designed metastructures are usually composed of elastic rubber films fixed to rigid edges, and a tension process is necessary before a small weight of mass is added to the films.⁷ The local resonance mechanism makes the metastructure cell behave like an independent oscillator, and multiple locally resonant metamaterial cells can be further assembled as a panel for enhanced sound isolation and large-scale applications.⁸ However, from the engineering point of view, the ductile

¹School of Automation, Nanjing University of Posts and Telecommunications, Nanjing, P.R. China

²School of Telecommunications and Information Engineering, Nanjing University of Posts and Telecommunications, Nanjing, P.R. China

³Structural Mechanics and Coupled Systems Laboratory, Conservatoire National des Arts et Metiers (CNAM), Paris, France

Corresponding author:

Ming Yuan, Nanjing University of Posts and Telecommunications, No. 9 Wenyuan Road, Xianlin, Nanjing 210023, P.R. China.

Email: yuanming@njupt.edu.cn



nature of the rubber film causes durability issues during deployment. In addition, the tension process increases the fabrication cost, and the tension variation introduces great uncertainties into the fabricated unit's natural frequencies.⁹

The incident sound energy can be harvested rather than dissipated, which makes the investigation of the acoustic metastructure's energy harvesting ability a very interesting issue. The converted electrical energy can be further stored and utilized by low-power electronic devices, which have broad application prospects for the Internet of Things. It should be noted that although acoustic energy harvesting (AEH) can be efficiently realized within the thermo-acoustic tube,¹⁰ such mechanism is not included in this study, and the excitation source is assumed as pure acoustic.

Following previous relevant acoustic energy harvesting studies, we find that acoustic resonators are usually introduced to amplify the incident sound pressure, such as the Helmholtz resonator¹¹ or quarter-wavelength resonator,¹² showing bulky for low-frequency applications. Metamaterial inspired energy harvesting studies have been initialized in recent studies, but the reported frequencies are located in the mid to high range.^{13,14} Only few research works in the low-frequency range are reported in recent years, adopting the piezoelectric mechanism¹⁵ or electromagnetic mechanism,¹⁶ the structural parameter influences on the system's vibro-acoustic properties and energy harvesting performance are not fully reported. Recently, a coiled-up metamaterial cavity is proposed to introduce sound pressure amplification, and stepped proof mass is introduced to improve the piezoelectric plate's energy harvesting performance within the cavity.¹⁷

In summary, little research work has been carried out with respect to metastructure-based low-frequency acoustic energy harvesting. The influence of the structural parameters on energy harvesting and vibro-acoustic properties has not been well reported.

In this paper, a durable acoustic metastructure is proposed, which can achieve both effectively low-frequency noise isolation and energy harvesting capabilities. Compared with the rubber film-based acoustic metastructure, the substrate is replaced by metallic material, and its durability is greatly improved. A piezoelectric patch and a proof mass are added to the substrate, and the finite element method is used to investigate the local resonant structural properties.

A sample acoustic metastructure model is described in the next section for the computational model setup. Then the sample's general vibro-acoustic properties are briefly depicted. The parameters' influences, such as the excitation sound pressure, the shape of the proof mass and substrate thickness and material's influence on the sample, are investigated next. A favorable configuration is selected for experimental verification. The experimental system was set up, and the relevant measured results are given in the Experimental demonstration section.

Acoustic metastructure sample model description

From previous studies, it is known that a rubber film-based substrate requires tension to give the film sufficient stiffness, and the dynamic characteristic of the membrane film is very sensitive to the tension value. This shortcoming can be overcome via increasing the substrate's Young's modulus. Here, a metallic substrate is used, and the tension process can be eliminated.

As shown in Figure 1, the proposed metamaterial structure is composed of three parts. The base part is a circular membrane. The middle part is a circular piezoelectric PZT-5H patch and the top part is a cylinder proof mass.

The three components are bonded centrally and the corresponding parameters are given in Table 1. According to these structural parameters, the calculated total weight of the sample is 17.6 g. The air speed is set to 343 m/s, and the air density is set to 1.29 kg/m³. The structural loss factor is defined as 0.04.

The PZT-5H's compliance matrix at constant electric field is

$$\mathbf{S}^E = \begin{bmatrix} 16.5 & -4.78 & -8.45 & 0 & 0 & 0 \\ -4.78 & 16.5 & -8.45 & 0 & 0 & 0 \\ -8.45 & -8.45 & 20.7 & 0 & 0 & 0 \\ 0 & 0 & 0 & 43.5 & 0 & 0 \\ 0 & 0 & 0 & 0 & 43.5 & 0 \\ 0 & 0 & 0 & 0 & 0 & 42.6 \end{bmatrix} \times 10^{-12} \text{ m}^2/\text{N}$$

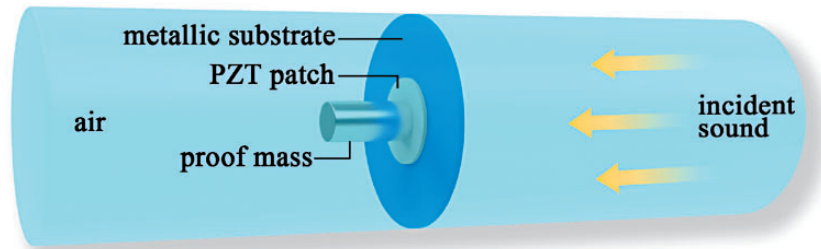


Figure 1. Schematic diagram of the proposed metamaterial structure.

Table 1. Component parameters of the metastructure.

Component	Radius (mm)	Thickness (mm)	Material	Density (kg/m ³)
Metallic substrate	37	0.2	Copper	8960
PZT-5H patch	15	0.2	Piezoelectric	7500
Proof mass	4	22.5	Structural steel	7850

The PZT-5H's direct piezoelectric coupling matrix is

$$\mathbf{d} = \begin{bmatrix} 0 & 0 & 0 & 0 & 741 & 0 \\ 0 & 0 & 0 & 741 & 0 & 0 \\ -274 & -274 & 593 & 0 & 0 & 0 \end{bmatrix} \times 10^{-12} \text{ C/N}$$

The PZT-5H's relative permittivity matrix under constant stress is

$$\boldsymbol{\epsilon}_r^T = \begin{bmatrix} 3130 & 0 & 0 \\ 0 & 3130 & 0 \\ 0 & 0 & 3400 \end{bmatrix}$$

Here, the COMSOLTM finite element software is adopted, and the numerical model is solved via frequency analysis. A clamped boundary condition is set at the edges of the circular substrate and is placed inside an acoustic tube, with a total length of 200 mm. The excitation source is plane acoustic wave, and radiation acoustic boundaries are used at the tube's two terminals, which makes the transmitted sound wave propagate in the downstream without reflection. Other acoustic boundaries are assumed as rigid walls.

For the mechanical domains (substrate, piezoelectric patch, and proof mass), the finite element meshes are generated using the swept method. With respect to the acoustic domain, meshes are generated using the free tetrahedral method. The minimum structural element size is 0.04 mm and the maximum structural element size is 4 mm. The minimum acoustical element size is 0.04 mm and the maximum acoustical element size is 4 mm. The total number of elements is around 42,407.

The acoustic–structure interface is added into the model to solve this fluid–structural interaction problem. The electrostatics and electrical circuit interfaces are also added into the model, which are used to simulate the piezoelectric effect and the current flowing to peripheral electrical circuit. The calculated electrical power value is essential for the energy harvesting performance evaluation and optimization.

The finite element analysis is performed in the frequency range of 20 Hz–1500 Hz. The incident sound pressure is 10 Pa, which means the sound pressure level (SPL) equals 114 dB. The piezoelectric patch is connected by a 10 k Ω resistor, which is found to provide the optimum resistance as discussed in the Parameter influences on acoustic energy harvesting section.

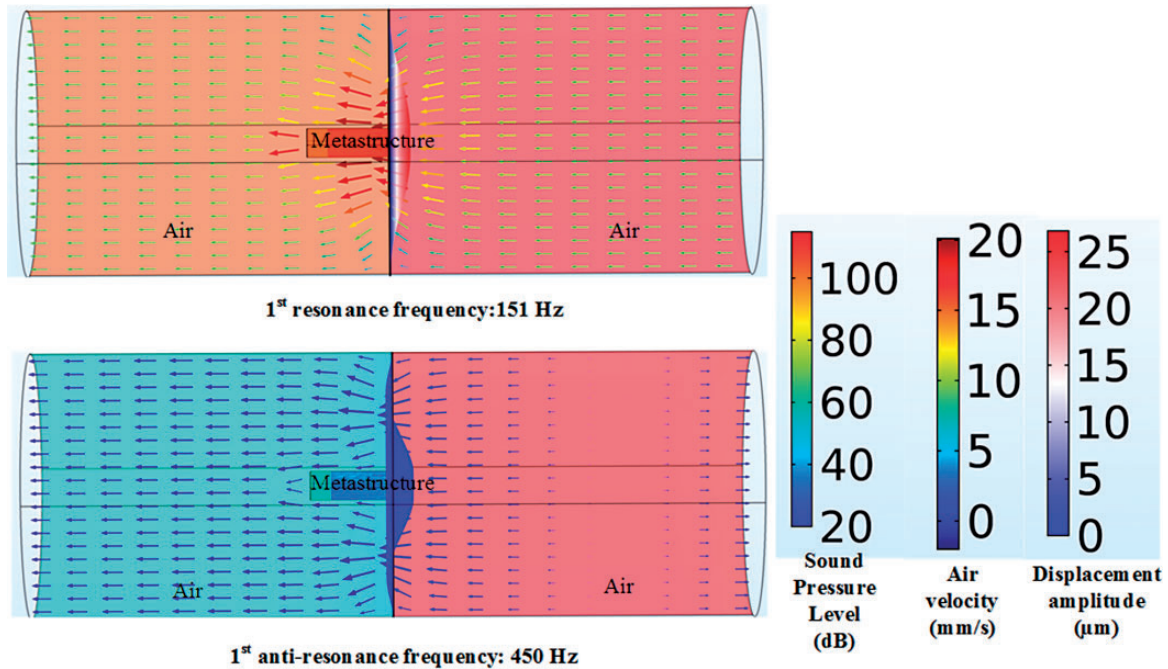


Figure 2. Vibro-acoustic properties of the sample at interesting frequencies.

Vibro-acoustic characteristics of the metastructure sample

Vibro-acoustic properties at the resonant and anti-resonant frequencies

For the local resonant acoustic metamaterial unit, previous studies have shown that the sound transmission dip occurs around the first resonant frequency and is mainly governed by structural damping. The sound transmission peak occurs near unit's first anti-resonance frequency.^{6,7}

For the numerical model in this study, the calculated first resonant frequency occurs at 151 Hz and the first anti-resonance frequency occurs at 450 Hz. Correspondingly, the sample's sound pressure distribution, air velocity, and structural displacement are presented in Figure 2.

The background color inside the tube (air domain) represents the SPL distribution; the color of arrows represents the magnitude of air velocity. The proposed metastructure is located in the figure's middle part, and its movement is represented using displacement amplitude.

It is shown at the first resonant frequency, the maximum structural displacement can be up to 25 μm . The air velocity value represented by the arrow reaches 20 mm/s. In contrast, at the first anti-resonant frequency, the maximum displacement reduces sharply and is only 0.48 μm . The small amount of structural displacement makes the metastructure behave very rigidly, which is suitable for sound insulation. Meanwhile, the transmitted sound velocity is also reduced sharply to only 0.06 mm/s, indicating that the transmitted sound energy is very small.

Effective dynamic mass density characteristics

To gain further insight into the sound transmission property, we examine the structure's effective dynamic mass density, which is defined as⁶

$$\rho_{eff} = (p_{in} - p_{out})/a_{nor} \quad (1)$$

where p_{in} is the averaged surface incident pressure, p_{out} is the averaged surface transmitted sound pressure, and a_{nor} is the averaged normal acceleration of the structure.

The calculated effective dynamic mass density is given in Figure 3.

As shown in Figure 3, the ρ_{eff} is a negative value below the first resonant frequency. Around the first resonant frequency, the ρ_{eff} value is zero, and it then becomes gradually larger before it comes to the maximum value.

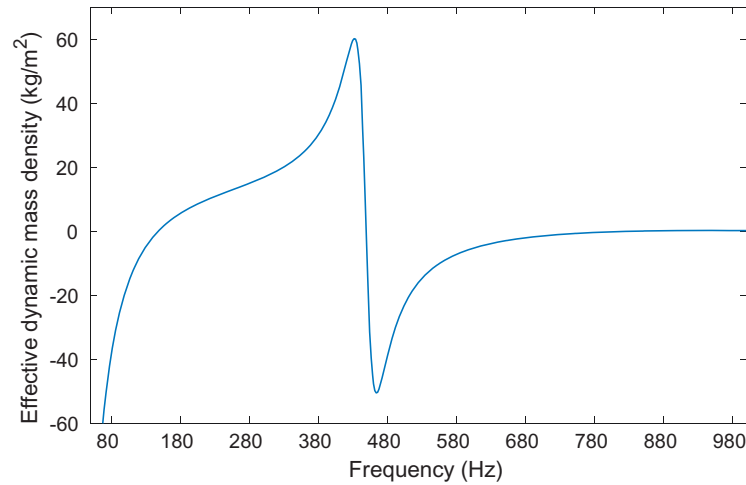


Figure 3. Effective dynamic mass density of the sample.

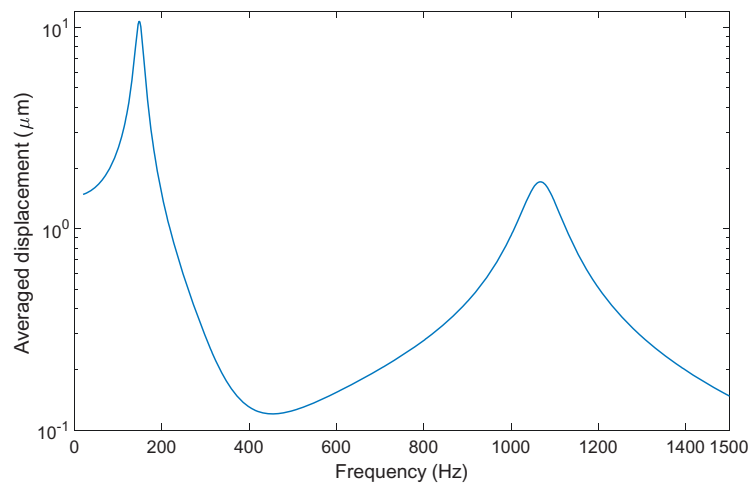


Figure 4. Average displacement of the substrate in vertical direction.

Above the largest point, it becomes divergent and drops sharply into negative territory. The negative dynamic mass property makes the transmitted sound decay exponentially, which prohibits far-field sound radiation. The large effective mass density makes the structure behave very stiff and causes the average displacement to have a very small value, causing strong sound transmission loss consequently. The average displacement of the substrate in the metastructure's vertical direction is shown in Figure 4, which demonstrates this phenomenon clearly.

Parameter influences on acoustic energy harvesting

Optimal resistance determination

To obtain the maximum amount of harvested power, the external circuit resistance value should be tuned to match the generator's source impedance. The output voltage and the corresponding calculated power with load resistance variation at the structural resonance frequency are shown in Figure 5.

The identified optimum resistance is 10 k Ω , and the harvest power is achieved at the maximum value under this condition.

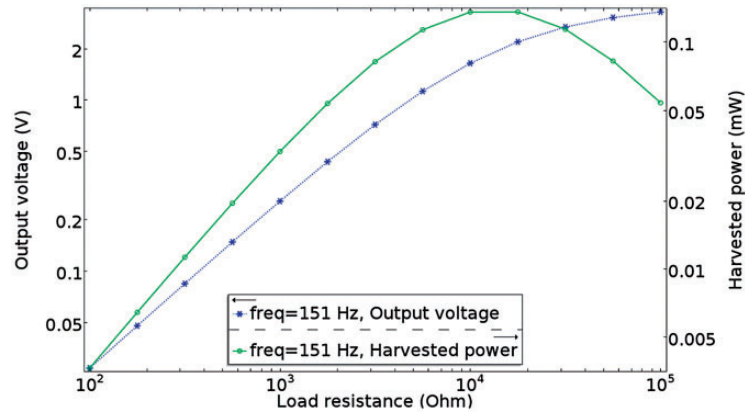


Figure 5. Output voltage and harvested power under different load values.

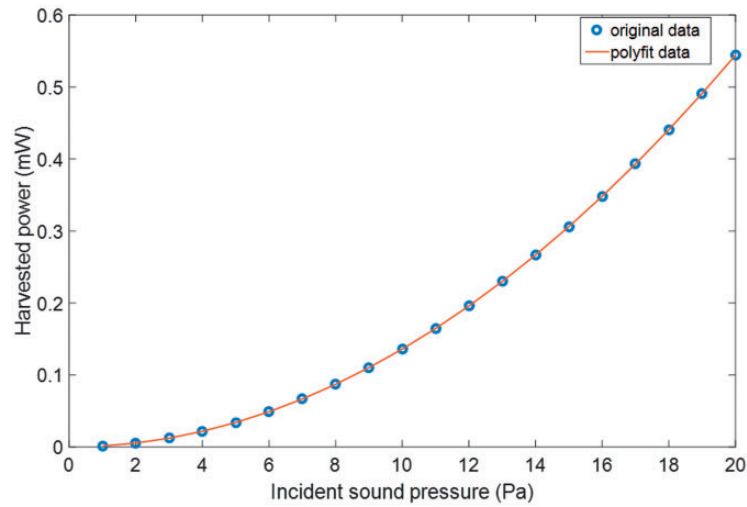


Figure 6. Harvested power as a function of incident sound pressure.

The influence of incident sound pressure

Figure 6 shows harvested electrical power value versus the incident sound pressure and the corresponding curve fitting result.

It is shown that the harvested power increases quadratically with the incident sound pressure, which has been disclosed in an analytical study.¹⁸

In this study, the polynomial curve fitting equation is

$$Pow = 0.0014p^2 \quad (2)$$

where Pow is the harvested power and p is the incident sound pressure.

The quadratic relation obeys the physical law, which can be deduced as follows.

Assuming the incident sound pressure is p , specific acoustic impedance is Z , the particle velocity v can then be represented as

$$v = \frac{p}{Z} \quad (3)$$

Table 2. Proof mass geometrical parameters.

Configuration	Radius (mm)	Height (mm)	Material
Proof mass 1	4	22.5	Structural steel
Proof mass 2	6	10	Structural steel
Proof mass 3	8	5.6250	Structural steel
Proof mass 4	10	3.6	Structural steel

where the constant number Z is the product of air density and sound speed.

The sound intensity I can be represented as

$$I = p \cdot v = \frac{p^2}{Z} \quad (4)$$

Accordingly, the incident sound power P_{in} can be represented as

$$P_{in} = I \cdot A = \frac{p^2 \cdot A}{Z} \quad (5)$$

where A is the sample's area, which is normal to the incident direction. Assuming the system's behavior is linear, the harvested power will be in proportion with the incident sound power and is in quadratic relation with the incident pressure.

If the incident power is too large, causing the system to exhibit strong non-linear dynamic properties, the above relation should be reconsidered.

The influence of the shape of the proof mass

The added parameters of the proof mass shape at the metastructure's center can also influence the energy harvesting performances. Here, the proof mass samples are assumed to have a cylinder shape with the same mass value.

Four geometric configurations are considered, and the variation is achieved by changing the cylinder's radius and height parameters. The detailed geometrical values are given in Table 2. In this simulation, the proof mass' volume size is set at 360 mm³, and the mass weight is 8.87 g.

As shown in Figure 7, the simulation result shows that for a given proof mass weight, the mass' geometric parameters can influence the harvested power significantly. At the first resonance frequency, the largest power value is 0.14 mW (smallest radius cylinder), and the smallest power value is 0.09 mW (largest radius cylinder). The discrepancy is as much as 56%.

This reason for this is that when the piezoelectric patch is bonded with proof mass, the bonding surface covered by the proof mass will not generate strain under sound wave excitation, and consequently no electrical charge is generated. Therefore, a larger radius proof mass has adverse effect on the energy harvesting power value.

However, the mass' radius cannot be infinitely small. One important reason is that for the same weight, a smaller radius will bring about a larger height, making the overall system less compact; another reason is that when the radius is small enough, the concentrated stress can exceed the piezo patch's bearing limit, causing material fracture and failure.

The influence of substrate materials

To investigate the substrate influence on energy harvesting performance, three different materials are considered: aluminum, copper, and high-strength alloy steel. These material properties are given in Table 3.

The structural loss factor η is defined as 0.04 in default, which is followed as in literature.^{19,20} This damping value is reasonable for energy harvesting devices that are piezoelectric based.

The substrate thickness is kept to be 0.2 mm with different materials and the obtained harvested power is shown in Figure 8.

For small structural loss value around the resonance frequency, the damping ratio ξ and the structural loss factor η have the relation of $\eta = 2\xi$. When the damping ratio is low, more electrical power will be generated at the resonance frequency. On the other hand, the system has a lower quality factor when the damping ratio is

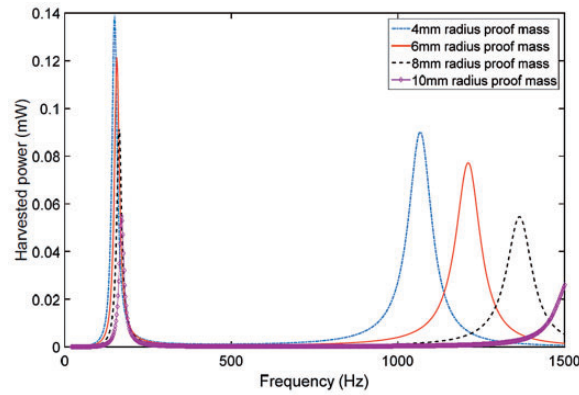


Figure 7. Effect of the proof mass shape on harvested power.

Table 3. Substrate material properties.

Material type	Young's modulus (GPa)	Poisson's ratio	Density (kg/m ³)
Aluminum	70	0.33	2700
Copper	110	0.35	8960
High-strength alloy steel	200	0.30	7850

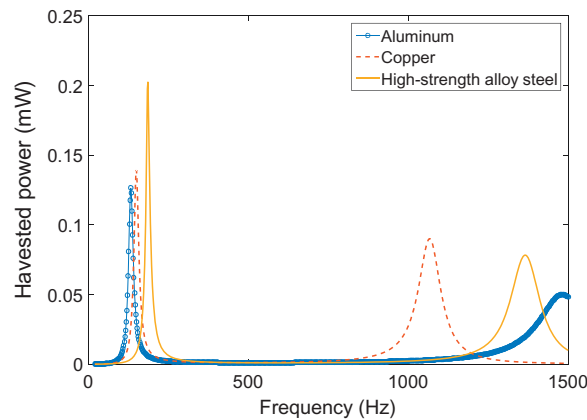


Figure 8. Harvested power with different substrate materials.

increased, resulting in a lower amount of harvested electrical power. For the first mode, the harvested power with different damping ratios of alloy steel substrate is shown in Table 4.

The influence of substrate thickness

Figure 9 shows the influence of substrate thickness on the harvested power.

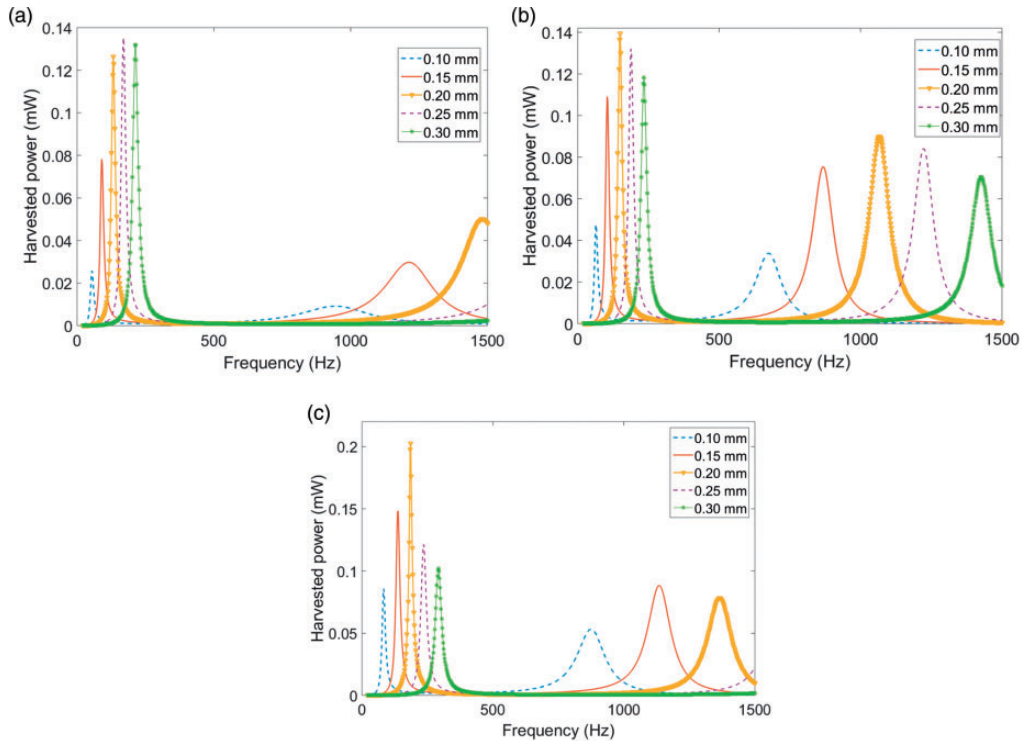
The simulation result indicates that to generate maximum power, there exists an optimal thickness ratio between the piezo patch and the substrate material. Here, the piezo patch's thickness is kept to be 0.2 mm and the substrate thickness is varied from 0.1 mm to 0.3 mm with 0.05 mm step.

The resonance frequency can be changed during the thickness variation. For plate type structure, the flexural rigidity D can be expressed as

$$D = \frac{Eh^3}{12(1 - \nu^2)} \quad (6)$$

Table 4. Harvested power for different damping ratios.

Damping ratio ξ	0.01	0.02	0.03	0.04	0.05
Harvested power (mW)	0.33	0.20	0.15	0.11	0.08

**Figure 9.** Variation of harvested power with different substrate thicknesses: (a) aluminum substrate, (b) copper substrate, and (c) high-strength alloy steel substrate.

where h is the plate's thickness, E is Young's modulus, and ν is Poisson's ratio. Hence, when the structure's thickness is kept as constant, a larger Young's modulus indicates that the structure is more stiff, generating a higher resonance frequency. On the other hand, when Young's modulus is determined and the thickness of plate is increased, the flexural rigidity becomes larger, generating a higher resonance frequency.

Meanwhile, impedance matching is optimized for the first mode, and the load resistance is determined according to the following equation²¹

$$R = \frac{1}{C_p \omega} \quad (7)$$

where C_p is the piezo patch's inherent capacitance and ω is the interesting angular frequency.

The calculated load resistance values for different simulation cases are shown in Table 5.

At the first resonance frequency, the optimal thicknesses for the aluminum, copper, and high-strength alloy steel substrates are 0.25 mm, 0.2 mm, and 0.2 mm, respectively. Among the optimum values, the 0.2-mm thick high-strength alloy steel substrate generates the largest output power (0.2 mW), which is 46.8% higher than the aluminum substrate optimal case and 42.8% higher than the copper substrate optimal case. The energy conversion efficiency can reach 20% for the 0.2-mm thick high-strength alloy steel substrate case.

The effective electromechanical coupling factor determines the effectiveness of piezoelectric energy harvester. As shown in previous studies, the effective electromechanical coupling factor is influenced by the thickness ratio and Young's modulus ratio of piezoelectric patch and substrate.^{22,23}

Table 5. Load resistance values in the simulation.

Substrate thickness (mm)	0.10	0.15	0.20	0.25	0.30
Load resistance (k Ω) (aluminum substrate)	27.7	16.6	11.3	8.8	7.0
Load resistance (k Ω) (copper substrate)	23.4	14.4	10.0	7.9	6.3
Load resistance (k Ω) (alloy steel substrate)	18.3	11.0	8.1	6.3	5.0

When the substrate thickness value is too small, the neural axis of the composite structure will move into the piezoelectric layer, which introduces electrical charge cancellation and generates little electrical power and very low effective electromechanical coupling factor.

When the substrate thickness is increased, the neutral axis will be located in the substrate layer gradually, indicating the charge cancellation is alleviated, and larger electrical power is obtained.

Correspondingly, as shown in Figure 9, for different substrate cases, the harvested power is increased before it achieves a maximum value. Meanwhile, for different substrate material with the same thickness, it has been shown that the substrate with larger Young's modulus generates a larger electrical power. This is attributable to the fact that the neutral axis is farther away from the piezoelectric layer, resulting in less charge cancellation and higher electromechanical coupling factor.

When the substrate thickness is further increased, the vibration response of the structure plays a more important role – the generated electrical power is related not only to the distance of the neural axis but also to the deflection of the structure. Therefore, when the substrate thickness increases to a certain extent, this latter factor plays a more important role. During the process, there exists an optimal thickness for the substrate, which corresponds to the maximum power.

As shown in Figure 9, the generated electrical power drops when the substrate thickness is further increased over the optimal thickness. Here, the steel substrate case drops more quickly owing to the larger stiffness causing the deflection to decrease more quickly, which corresponds to a sharper electrical power drop off.

Experimental demonstration

According to the previous simulation analysis given in the Parameter influences on acoustic energy harvesting section, the 0.2-mm thick high-strength alloy steel, 4-mm radius proof mass, and 0.2-mm thick PZT-5H configuration provides the maximum harvested power value. Therefore, this configuration is chosen for the following experimental study. The fabricated components are weighted on a precise scale and the measured total weight is 17.02 g, which has a gram bias of only 0.58 compared to the theoretical prediction.

Figure 10(a) shows the photograph of experimental system for the metastructure's performance evaluation. The corresponding schematic diagram is given in Figure 10(b).

In the experimental system, an NI PXI-4461 AO channel (24 bits) provides a programmable signal to an audio power amplifier, which then drives a 5.5-inch loudspeaker (HiVi F5). An acrylic tube (length 1 m, thickness 8 mm, inner radius 77 mm) is used for plane sound wave propagation. To generate plane sound waves, the excitation frequency should be below the tube's cutoff frequency, which is about 1300 Hz. A fixture unit was designed and fabricated, which helps to affix the metastructure to acrylic tube. PattexTM super glue was used to bond the proof mass to the center of the PZT-5H patch. The PZT-5H patch was further bonded to the center of the disk's center.

The incident sound pressure was measured using a G.R.A.S 40 PP microphone sensor (sensitivity 51 mv/Pa), and it was sampled by the NI PXI-4461 AI channel (24 bits). The SPL was calculated with the help of LabVIEWTM sound and vibration measurement suite. The harvester's output voltage was measured by the NI PXI-6361 AI channel (16 bits).

A band limited white noise (20 Hz–1000 Hz) is used as the excitation signal, which is generated by the NI-DAQ system and is amplified by the audio power amplifier to drive the loudspeaker. A microphone sensor (at the tube's end) is used to measure the excitation sound pressure and the acquired signal is analyzed via LabVIEW sound and vibration measurement suite. The measured result is shown in Figure 11(a).

According to Figure 11(a), the sound spectrum is not uniform. This can be caused by many factors, such as speaker's dynamic properties, ambient surrounding supports.

Secondly, the fabricated sample's frequency property is measured. The test structure is mounted at the tube's end, and the band-limited stochastic acoustic sound wave is used as the excitation source. Due to the piezoelectric effect, the piezoelectric patch's voltage can be acquired to reveal the structure's frequency property.

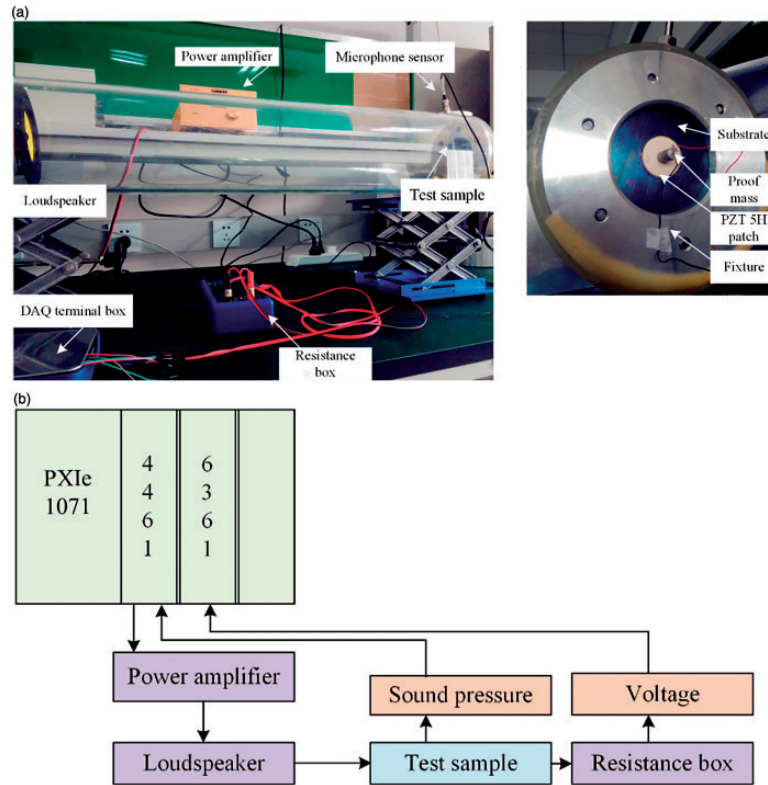


Figure 10. Experimental system setup. (a) Photograph of the experimental system. (b) Schematic diagram of the experimental system.

The measured frequency response is shown in Figure 11(b). It is shown that in the band of 100–200 Hz, although the acoustic excitation is weak, due to the metastructure's local resonance property, a large voltage peak can be found. At the higher frequency band (200 Hz–1000 Hz), the incident energy is much larger than the previous low-frequency band, which causes the structure to be strongly excited than the low-frequency band. Besides, there are also some voltage peaks at high frequencies, and these peaks have close relation with the incident sound spectrum.

The measured first resonance frequency occurs at 155 Hz, whereas the simulated result corresponding to steel substrate occurs at 185 Hz. This difference can be caused by the non-perfect clamping condition. As shown in Figure 12, the metallic substrate is mounted on a pair of rims, and six bolts are used to generate clamping force to the edge of the sample.

Theoretically, when the boundary condition is assumed as clamped, the deflection and derivative of the edge are zero. As the support rim cannot be perfectly rigid, this boundary condition is actually an idealized assumption. For a realistic experimental study, the relaxed clamped boundary condition makes the resonance frequency of the sample lower than the idealized perfect clamped boundary condition.²⁴

At the first resonance frequency, the incident SPL is kept at 114 dB (10 Pa), and the harvester's output voltage versus load resistance is shown in Figure 13.

According to equation (8), the corresponding harvested power value Pow versus load resistance R_{load} can be calculated as²⁵

$$Pow = V_{pp}^2 / 8R_{load} \quad (8)$$

where V_{pp} is the peak-to-peak voltage on the resistance load.

The corresponding result is plotted in Figure 14.

The experimental result shows that 0.21 mW maximum electrical power can be harvested. The measured power has almost the same value as predicted by the numerical simulation. The incident acoustic power is 1 mW; therefore, the acoustical–electrical conversion efficiency is 21%.

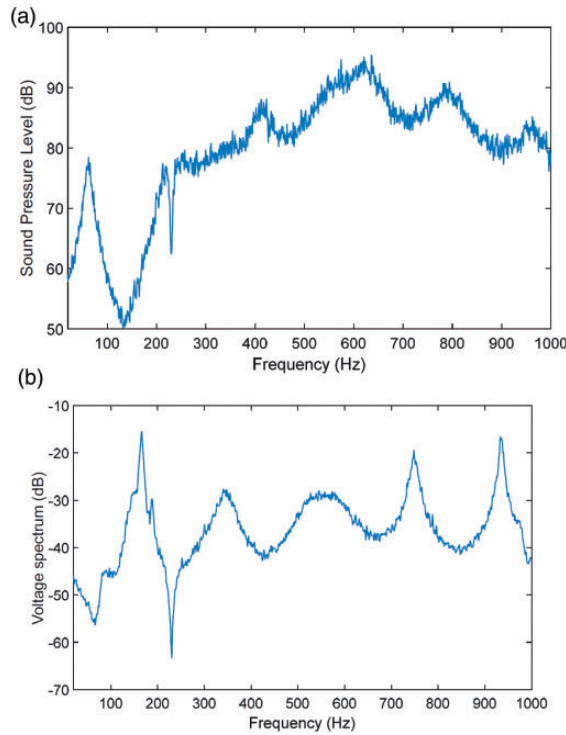


Figure 11. Incident sound spectrum and corresponding generated voltage spectrum. (a) Incident sound wave frequency properties. (b) Generated voltage spectrum from the piezoelectric path.

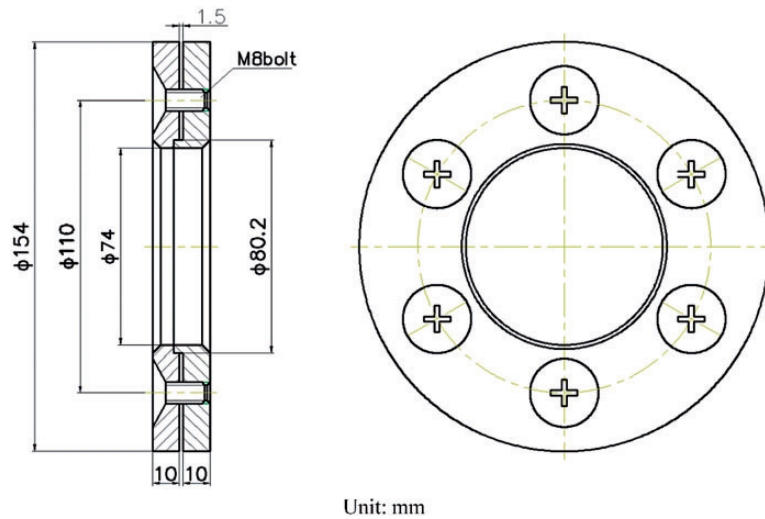


Figure 12. Schematic diagram of the fixture apparatus.

To further improve the electrical conversion performance, it would be favorable to boost the piezoelectric material’s performance. The reason is that for the piezoelectric 31 mode energy harvesting application, the corresponding electromechanical coupling factor k_{31} can be written as

$$k_{31} = \frac{d_{31}}{\sqrt{s_{11}^E \epsilon_{33}^T}} \tag{9}$$

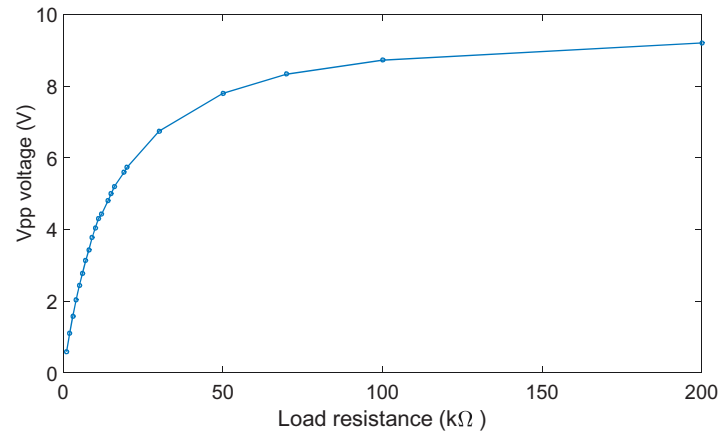


Figure 13. Harvester's output voltage versus load resistance.

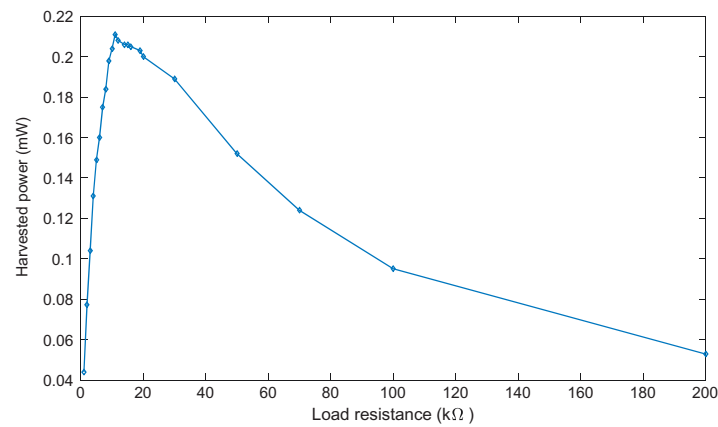


Figure 14. Harvester's output power versus load resistance.

where d_{31} is the charge on surface normal to three-axis, which is caused by the applied stress along one-axis; s_{11}^E is the compliance under constant electric field; and ϵ_{33}^T is the permittivity under constant stress.

According to equation (9), a large value of d_{31} is favorable to have a higher electromechanical coupling factor k_{31} . For instance, the recently developed PMN-PT, PZN-PT single crystals have superior piezoelectric performance compared with the commonly used PZT material. Hence, adopting this type of materials shows improved energy harvesting performance, which has recently been demonstrated by experimental studies.^{26,27}

With respect to the sample's strength, the PZT-5H patch is the system's most fragile part. The PZT-5H material is easy accessible, possessing satisfying piezoelectric properties and low fabrication cost, these merits make it being extensively used in the piezoelectric energy harvesting studies. However, as it belongs to ceramic category, it has the brittle drawback and cannot bear large substrate deformation. This drawback limits its application under severe mechanical excitation. For the acoustic energy harvesting (AEH) application, as the energy intensity is usually not strong enough, the proposed structure's durability can be guaranteed.

As a single metastructure cell's harvested power value can reach 0.21 mW, it would be very interesting to fabricate multiple cells as a meta-plate for large electrical power generation, and we are confident that this work will be carried out in the near future.

Conclusion

In this study, a metastructure with both noise isolation and energy harvesting abilities is proposed. Compared with the rubber-based substrate, metallic-based substrate can omit the tension process and provide stronger durability for practical engineering application. The structural parameter's influence on the sample's

vibro-acoustic properties and energy harvesting performance are investigated via the finite element method. Simulation results indicate that the incident sound wave intensity, the shape of the proof mass, the type of substrate material, and the thickness of the substrate all have substantial influence on the metastructure. The configuration with the best energy harvesting ability is also testified through experimental study, which shows competitive performance comparing with previous AEH studies.

Substantial noise isolation at the first anti-resonance frequency and efficient acoustic energy harvesting at the first resonant frequency can be achieved via the proposed metastructure. Although at the efficient energy harvesting frequency, the corresponding sound isolation performance nearby can be unsatisfying. This drawback could be overcome if multiple layers' configuration is adopted, where each layer has different local resonant property, improving the overall sound isolation performance and broadening the energy harvesting frequency band. The proposed multi-functional metastructure provides new insights for acoustic energy manipulation and utilization. These analysis results may be used as guidance for further metastructure-based acoustic energy harvesting studies.

Acknowledgments

The authors sincerely thank the reviewers and editor for their valuable comments and suggestions that have led to the present improved version.


Declaration of conflicting interests

The author(s) declared no potential conflicts of interest with respect to the research, authorship, and/or publication of this article.

Funding

The author(s) disclosed receipt of the following financial support for the research, authorship, and/or publication of this article: This research was sponsored by the Natural Science Foundation of Jiangsu Province (Grant No. BK20160895), the National Natural Science Foundation of China (Grant Nos. 61372044, 61701250, 11604158), NUPTSF (Grant Nos. NY215009, 215032, 217029), and the Natural Science Foundation of the Jiangsu Higher Education Institutions of China (14KJA510002).

ORCID iD

Ming Yuan  <http://orcid.org/0000-0001-7209-0357>

References

1. Bansod PV, Teja TS and Mohanty AR. Improvement of the sound absorption performance of jute felt-based sound absorbers using micro-perforated panels. *J Low Freq Noise Vib Act Control* 2017; 36: 376–398.
2. Rakhshan M, Moula E, Shabani-Nia F, et al. Active noise control using wavelet function and network approach. *J Low Freq Noise Vib Act Control* 2016; 35: 4–16.
3. Bagha AK and Modak SV. Active structural-acoustic control of interior noise in a vibro-acoustic cavity incorporating system identification. *J Low Freq Noise Vib Act Control* 2017; 36: 261–276.
4. Li Y, Jiang X, Li RQ, et al. Experimental realization of full control of reflected waves with subwavelength acoustic metasurfaces. *Phys Rev Appl* 2014; 2: 1–11.
5. Li Y, Liang B, Gu Z, et al. Reflected wavefront manipulation based on ultrathin planar acoustic metasurfaces. *Sci Rep* 2013; 3: 2546.
6. Yang Z, Mei J, Yang M, et al. Membrane-type acoustic metamaterial with negative dynamic mass. *Phys Rev Lett* 2008; 204301: 1–4.
7. Naify CJ, Chang C, Mcknight G, et al. Transmission loss and dynamic response of membrane-type locally resonant acoustic metamaterials. *J Appl Phys* 2010; 108: 1–7.
8. Yang Z, Dai HM, Chan NH, et al. Acoustic metamaterial panels for sound attenuation in the 50-1000 Hz regime. *Appl Phys Lett* 2012; 96: 41906.
9. Ma F, Huang M and Wu JH. Ultrathin lightweight plate-type acoustic metamaterials with positive lumped coupling resonant. *J Appl Phys* 2017; 121: 10.
10. Zhao D and Chew Y. Energy harvesting from a convection-driven Rijke-Zhao thermoacoustic engine energy harvesting from a convection-driven Rijke-Zhao thermoacoustic engine. *J Appl Phys* 2012; 112: 1–7.
11. Liu F, Phipps A, Horowitz S, et al. Acoustic energy harvesting using an electromechanical Helmholtz resonator. *J Acoust Soc Am* 2008; 123: 1983–1990.

12. Li B, Laviage AJ, You JH, et al. Harvesting low-frequency acoustic energy using multiple PVDF beam arrays in quarter-wavelength acoustic resonator. *Appl Acoust* 2013; 74: 1271–1278.
13. Qi S, Oudich M, Li Y, et al. Acoustic energy harvesting based on a planar acoustic metamaterial. *Appl Phys Lett* 2016; 108: 263501.
14. Yang A, Li P, Wen Y, et al. Enhanced acoustic energy harvesting using coupled resonance structure of sonic crystal and Helmholtz resonator. *Appl Phys Express* 2013; 6: 127101.
15. Li J, Zhou X, Huang G, et al. Acoustic metamaterials capable of both sound insulation and energy harvesting. *Smart Mater Struct* 2016; 25: 45013.
16. Ma G, Yang M, Xiao S, et al. Acoustic metasurface with hybrid resonances. *Nat Mater* 2014; 13: 873–878.
17. Sun KH, Kim JE and Kim J, et al. Sound energy harvesting using a doubly coiled-up acoustic metamaterial cavity. *Smart Mater Struct* 2017; 26: 75011.
18. Kim S, Clark WW and Wang Q-M. Piezoelectric energy harvesting with a clamped circular plate: analysis. *J Intell Mater Syst Struct* 2005; 16: 847–854.
19. Roundy S, Wright PK and Rabaey JM. Vibration sources and conversion model BT. In: Roundy S, Wright PK and Rabaey JM (eds) *Energy scavenging for wireless sensor networks: with special focus on vibrations*. Boston, MA: Springer, pp. 27–39.
20. Orban F. Damping of materials and members in structures. *J Phys Conf Ser* 2011; 268: 12022.
21. Lu F, Lee HP and Lim SP. Modeling and analysis of micro piezoelectric power generators for micro-electromechanical-systems applications. *Smart Mater Struct* 2004; 13: 57.
22. Wang Q, Du X, Xu B, et al. Electromechanical coupling and output efficiency of piezoelectric bending actuators. *IEEE Trans Ultrason Ferroelectr Freq Control* 1999; 46: 638–646.
23. Cho J, Anderson M, Richards R, et al. Optimization of electromechanical coupling for a thin-film PZT membrane: I. Modeling. *J Micromech Microeng* 2005; 15: 1797–1803.
24. Gomes LT. Effect of damping and relaxed clamping on a new vibration theory of piezoelectric diaphragms. *Sensors Actuators A Phys* 2011; 169: 12–17.
25. Fang H-B, Liu J-Q, Xu Z-Y, et al. Fabrication and performance of MEMS-based piezoelectric power generator for vibration energy harvesting. *Microelectronics J* 2006; 37: 1280–1284.
26. Karami MA, Bilgen O, Inman DJ, et al. Experimental and analytical parametric study of single-crystal unimorph beams for vibration energy harvesting. *IEEE Trans Ultrason Ferroelectr Freq Control* 2011; 58: 1508–1520.
27. Yang Z and Zu J. Comparison of PZN-PT, PMN-PT single crystals and PZT ceramic for vibration energy harvesting. *Energy Convers Manag* 2016; 122: 321–329.